# A nonlocal kinetic model for predator-prey interactions

R. C. Fetecau * J. Meskas *

April 28, 2013

**Abstract**

We extend the aggregation model from [1] by adding a field of vision to individuals and by including a second species. The two species, assumed to have a predator-prey relationship, have dynamics governed by nonlocal kinetic equations that include advection and turning. The latter is the main mechanism for aggregation and orientation, which results from interactions among individuals of the same species as well as predator-prey relationships. We illustrate numerically a diverse set of predator-prey behaviours that can be captured by this model. We show that a prey's escape outcome depends on the social interactions between its group members, the prey's field of vision and the sophistication of the predator's hunting strategies.

**Keywords**: swarm dynamics, biological aggregations, predator-prey, field of vision
**AMS Subject Classification**: 92D25, 35Q92

## 1 Introduction

In recent years many mathematical models have been introduced in an attempt to describe collective behaviour in animal groups. Such biological aggregations are ubiquitous in nature, for instance flocks of birds [2], swarms of insects (mosquitoes, bees, locusts) [3], schools of fish [4], herds of ungulates and even crowds of humans. Research on models of animal group behaviour has been driven by pure scientific interest, as well as by their applications. For example, the fishing industry can benefit from more knowledge about fish behaviour [5]. Also, understanding swarming and flocking in nature can help improve robot communication [6] or coordination among autonomous vehicles [7]. Applications reach even seemingly unrelated disciplines such as social sciences and economics [8, Parts I and II].

More complex systems are those that involve multiple types of groups and interactions, such as intra-species competition for resources or inter-species predator-prey relationships. Regarding the latter, both predators and prey develop group strategies that, respectively, make the chase and escape more efficient. Some examples of multiple group behaviours are dolphins confining fish into a bait ball [9], wolves chasing white-tailed deer [10] and Eleonora's falcons' high diving speed technique to capture a bird in a flock [11].

*Department of Mathematics, Simon Fraser University, 8888 University Dr., Burnaby, BC V5A 1S6, Canada, email: {van,jmeskas}@sfu.ca

There are two main classes of mathematical models that are used to describe animal groups. The first is of Lagrangian type, which are particle-based models that consist of interaction rules governing the evolution of individuals as they interact with their neighbours [12]. Frequently, such models are expressed in terms of large systems of ordinary differential equations [13, 14]. This formulation captures, to reasonable precision, many real biological aggregations, but it does not allow for rigorous analysis and becomes computationally expensive for a large number of individuals.

The second class of models uses an Eulerian approach, where the problem is formulated as an evolution equation for the population density field. In many instances, such Eulerian models originate in fact from particle-based models, in the limit when the number of particles approaches infinity [15, 16, 17]. The dynamics in an Eulerian model is governed by a partial differential equation (PDE), which typically is nonlinear and nonlocal. PDE aggregation models can be further classified into kinetic/mesoscopic [18] and continuum/macroscopic [19, 20, 21]. Interest on both kinetic and continuum models for aggregation has grown very fast lately, either separately, or in connection, where corresponding hydrodynamic limits of kinetic models have been established and studied [15, 16, 22].

In this paper we consider the nonlocal kinetic model introduced and studied in [1], which represents the extension to two-dimensions of the hyperbolic model from [23, 24, 25]. The distinctive feature of these models is that they consider *turning* as the main mechanism for aggregation and self-collective behaviour. Individuals turn to respond to signals perceived from their neighbours. The models take into account *all* social interactions (attraction, repulsion, alignment) which exist among individuals in a group, interactions which are incorporated, via *nonlocal* terms, into the turning rates. They are zonal models, where responses to neighbours are modelled by interaction potentials (kernels) which delineate zones of repulsion, alignment and attraction acting at short, intermediate, and long ranges, respectively.

The present research extends the model from [1] in several directions: i) adds a field of vision to individuals, and ii) includes a second species and considers predator-prey interactions. Adding a field of vision produces a more realistic reaction behaviour of individuals since they cannot see behind themselves. Limited vision (or more general, sensorial perception) has been considered in other aggregation models [12, 26, 27, 28], and it was shown to be an essential feature, with important effects on the collective behaviour of the group. The addition of a predator gives another layer of complexity because biological aggregates do not live in isolation from other species and are subject to predation. Both extensions are added in consistency with the overall setup of the model from [1]. The field of vision is included via an additional kernel that truncates the contribution of the existing interaction kernels. The predator dynamics is modelled with a kinetic equation similar in form to the equation from [1], except that now turning of both prey and predator individuals results from interactions among individuals of the same species, as well as predator-prey relationships.

The literature on mathematical models for predator-prey interactions is vast and has a long history. Most of these models consist of a coupled system of ordinary differential equations describing the time evolution of the prey and predator densities. Typically, the models assume that, in the absence of the other species, the two densities have their own growth and death rates, while the interactions are included in terms that model the functional responses of one species with respect to the other. Such models are referred to as Kolmogorov-type equations. A recent book by Brauer and Castillo-Chavez [29] (Chapters 4-6) presents and discusses several models in this category, starting with the celebrated Lotka-Volterra model (1925). The models of this sort have become increasingly sophisticated over the years, with various forms of functional responses being studied [30]. Various

extra features have been considered too, such as harvesting and stocking [31], or dormant predators [32]. The analysis of these models mostly involve techniques from dynamical systems and bifurcation theory, where stability of fixed points or limit cycles is investigated, possibly in terms of a bifurcation parameter.

Spatial dependence in predator-prey dynamics is typically included via diffusion terms [33], and literature on such reaction-diffusion systems is also extensive (see [34] for a review). Much less represented are models of hyperbolic type. There exist a few hyperbolic predator-prey models which incorporate advection and reaction/competition terms, but studies on these models are limited to investigations of the traveling wave solutions [35, 36]. A major shortcoming of these PDE models is that they focus on how the predator-prey interactions affect the population sizes, but omit to consider basic predator-prey relationships such as predators' hunting techniques or prey's avoidance strategies. The nonlocal turning rates in our model consider such interactions between prey and predator, as well as interactions among individuals of the same group. For a better illustration of the role of turning in predator-prey interactions, we do *not* consider birth/death terms in this model. We want to emphasize in this work the formation of the biological groups and the hunting/escaping strategies rather than the long time behaviour of a predator-prey system where birth and death processes play a major role. Birth and death terms, as in [37] for instance, could be easily incorporated into our model and a full investigation of such an enhanced model is planned for future work.

The paper is organized as follows. Section 2 starts by presenting the aggregation model from [1], and then introduces the predator-prey model investigated in this article. Section 3 describes the numerical method used to generate the numerical results. Section 4 illustrates numerically a diverse set of predator-prey behaviours that can be captured with our model. As these animal behaviours depend on the sophistication of the predator, we present several cases: a stationary predator, a moving predator that does not respond to its surroundings, and a predator that turns and chases the prey.

## 2 Model description

In this section we first introduce the model from [1] and discuss its modelling assumptions, then present the two extensions which this paper is concerned with: adding a field of vision/blind zone, and including intra- and inter-species interactions.

### 2.1 Aggregation model from [1]

The model introduced in [1] is given by the following integro-differential equation

$$\partial_t u + \gamma \vec{e}_\phi \cdot \nabla_{\vec{x}} u = -\lambda(\vec{x}, \phi) u + \int_{-\pi}^{\pi} T(\vec{x}, \phi', \phi) u(\vec{x}, \phi', t) d\phi', \tag{1}$$

where $u$ is the population density of individuals at spatial location $\vec{x} = (x, y)$ and oriented in direction $\phi \in (-\pi, \pi]$, measured from the positive x-axis. The individuals are moving in the direction $\vec{e}_\phi = (\cos\phi, \sin\phi)$ with constant speed $\gamma$. The functions $\lambda(\vec{x}, \phi)$ and $T(\vec{x}, \phi', \phi)$ model the turning rates of individuals and are dependent on the individuals' attraction, repulsion and alignment with each other. The function $\lambda(\vec{x}, \phi)$ represents the rate at which individuals in state $(\vec{x}, \phi)$ turn, and $T(\vec{x}, \phi', \phi)$ describes the rate at which an individual located at $\vec{x}$ reorients itself

from $\phi'$ to $\phi$, due to interaction with neighbours. The modelling and the precise forms of the turning rates are presented later in this section.

In summary, the left-hand-side represents advection at constant velocity $\gamma$, and the right-hand-side contains loss and gain terms due to turning and changes of direction. There is an important consistency relation between the gain and loss terms, which ultimately assures conservation of mass. Namely, $\lambda(\vec{x},\phi)$, the turning rate from direction $\phi$ to *any* other direction, should be obtained by integrating $T(\vec{x},\phi,\phi')$, the turning rate from direction $\phi$ to $\phi'$, over all possible *new* directions $\phi'$:

$$\lambda(\vec{x},\phi) = \int_{-\pi}^{\pi} T(\vec{x},\phi,\phi')\, d\phi'. \tag{2}$$

Numerical simulations in [1] showed very rich dynamics and collective behaviour of solutions to model (1). Starting from random initial conditions, the following group formations in two dimensions were obtained: i) swarms (aggregation into a group, with no preferred direction of motion), and ii) parallel/ translational motion in a certain preferred direction with either uniform spatial density or aggregation into groups.

We present briefly below the modelling assumptions on the inter-individual interactions, and provide expressions for the turning rates $\lambda(\vec{x},\phi)$ and $T(\vec{x},\phi',\phi)$. For more details, the reader can consult [1].

**Factors of influence.** The model depicts an individual's decision to continue moving in its current direction or to turn based on its neighbours. We assume that the only two factors that influence turning are the distance from neighbours and the neighbours' orientation. Each factor is modelled mathematically by interaction kernels.

i. *Distance kernels.* Each individual is assumed to be surrounded by zones of repulsion, alignment, and attraction acting at short, intermediate and long ranges, respectively (see Figure 1(a)). These zones are modelled with distance kernels $K_j^d$:

$$K_j^d(\vec{x}) = \frac{1}{A_j} e^{-\left(\sqrt{x^2+y^2}-d_j\right)^2/m_j^2}, \qquad j = r, al, a, \tag{3}$$

where $j = r, al, a$, stands for repulsion, alignment, or attraction, respectively, $d_j$ represents the radius and $m_j$ the thickness of the respective influence zone (see Figure 1(a)). The $A_j$'s are normalizing constants that make the spatial integral of each kernel equal 1. These constants are given by:

$$A_j = \pi m_j \left( m_j e^{-d_j^2/m_j^2} + \sqrt{\pi} d_j \left(1 + \operatorname{erf}\left(d_j/m_j\right)\right)\right). \tag{4}$$

Figure 1(b) shows the attraction kernel $K_a^d$. Note that the three interaction zones may overlap.

ii. *Orientation kernels.* We discuss first the attractive orientation kernel. Suppose a decision making individual located at $\vec{x}$ is heading in direction $\phi$ and senses a neighbour located at $\vec{s}$, within its attraction zone — see Figure 2(a). The relative location $\vec{s}-\vec{x}$ makes an angle $\psi$ with the positive $x$ axis. Due to attraction, the reference individual makes a decision to turn in order to approach its neighbour at $\vec{s}$. The larger the difference $|\phi-\psi|$, the higher the likelihood of the decision making individual to turn. These considerations are included in the following attraction kernel [1] $K_a^o$:

$$K_a^o(\vec{s};\vec{x},\phi) = \frac{1}{2\pi}\left(-\cos\left(\phi-\psi\right)+1\right). \tag{5}$$

[1] Superscripts $d$ and $o$ in the interaction kernels refer to distance and orientation (angle), respectively. Subscripts $r, al, a$ stand for repulsion, alignment and attraction, respectively.

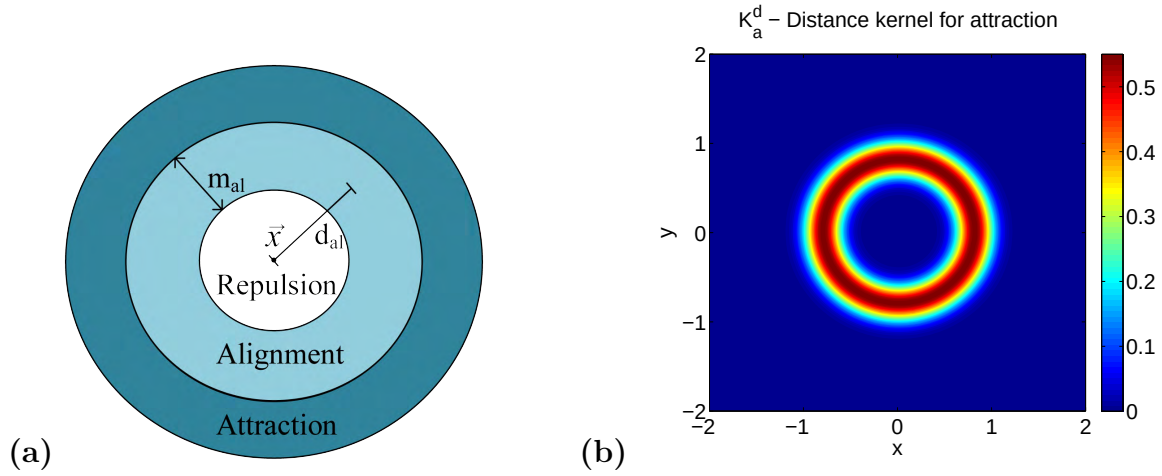


Figure 1: (a) Zones of repulsion, alignment and attraction. The radius and thickness of each zone is determined by $d_j$ and $m_j$, respectively, where $j = r, al, a$. (b) Generic contour plot of the attractive distance kernel $K_a^d$.

Note that $K_a^o$ is smallest when $\phi$ and $\psi$ are the same ($\vec{x}$ is already moving towards $\vec{s}$, hence no need to turn), and largest when $\phi$ and $\psi$ are an angle of $\pi$ away from each other ($\vec{s}$ is directly behind $\vec{x}$). Referring again to Figure 2(a), $\vec{x}$ is more likely to turn because of the attractive influences of $\vec{s'}$ compared to $\vec{s}$. The $\frac{1}{2\pi}$ factor renormalizes the kernel so it integrates to 1.

Very similar considerations can be made regarding the change of orientation due to repulsion. The repulsion kernel, $K_r^o$ has the expression:

$$K_r^o\left(\vec{s};\vec{x},\phi\right) = \frac{1}{2\pi}\left(\cos\left(\phi-\psi\right)+1\right). \tag{6}$$

Compared to (5), (6) has change of sign in front of the cosine term, which reverses the likelihood of turning.

Finally, regarding the alignment orientation kernel, we refer to Figure 2(b). The decision making individual is located at $\vec{x}$ and is moving in direction $\phi$. A neighbour $\vec{s}$ located in its alignment range moves in direction $\theta$. The larger the relative orientation $|\phi-\theta|$, the higher the likelihood of the reference individual to turn to align with its neighbour. Similar to previous considerations, this is encoded in the following function:

$$K_{al}^o\left(\theta,\phi\right) = \frac{1}{2\pi}\left(-\cos\left(\phi-\theta\right)+1\right). \tag{7}$$

The six kernels from Equations (3), (5), (6) and (7) are the building blocks for both turning rate functions $\lambda$ and $T$. The development of these two functions are discussed below.

**Turning rate $\lambda(\vec{x},\phi)$.** The turning rate $\lambda(\vec{x},\phi)$ is assumed to take contributions from all three social interactions:

$$\lambda(\vec{x},\phi) = \lambda_a(\vec{x},\phi) + \lambda_r(\vec{x},\phi) + \lambda_{al}(\vec{x},\phi), \tag{8}$$

where each component $\lambda_j$ $(j = r, al, a)$ is defined in terms of the distance and orientation kernels introduced above.

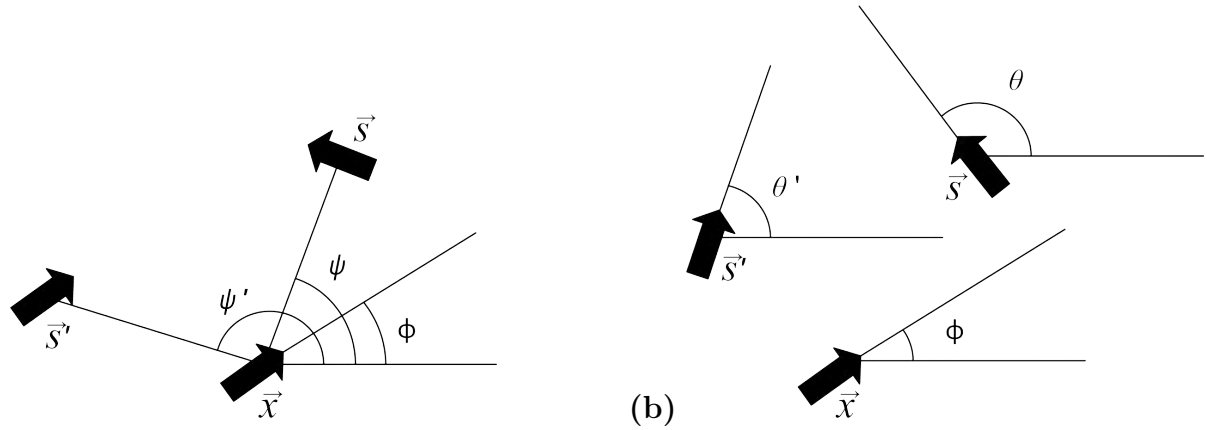


Figure 2: Change of orientation due to interaction with neighbours. The decision making individual is located at $\vec{x}$ and is moving in direction $\phi$. (a) Attraction. The reference individual at $\vec{x}$ is more likely to turn due to its interaction with $\vec{s'}$ than with $\vec{s}$, as $|\phi - \psi'| > |\phi - \psi|$. (b) Alignment. The individual at $\vec{x}$ is more likely to turn due to its interaction with $\vec{s}$ than with $\vec{s'}$, as $|\phi - \theta| > |\phi - \theta'|$.

The attraction turning rate $\lambda_a$ is given by the expression:

$$\lambda_a(\vec{x}, \phi) = q_a \int_{\mathbb{R}^2} \int_{-\pi}^{\pi} K_a^d(\vec{x} - \vec{s}) K_a^o(\vec{s}; \vec{x}, \phi) u(\vec{s}, \theta, t) d\theta d\vec{s}, \tag{9}$$

where $q_a$ is a constant that represents the strength of attraction. The integral in the right-hand-side is taken over $\vec{s}$ and $\theta$, which accounts for all neighbours' positions and directions, respectively.

The other two components of $\lambda$ are defined similarly:

$$\lambda_r(\vec{x}, \phi) = q_r \int_{\mathbb{R}^2} \int_{-\pi}^{\pi} K_r^d(\vec{x} - \vec{s}) K_r^o(\vec{s}; \vec{x}, \phi) u(\vec{s}, \theta, t) d\theta d\vec{s}, \tag{10}$$

$$\lambda_{al}(\vec{x}, \phi) = q_{al} \int_{\mathbb{R}^2} \int_{-\pi}^{\pi} K_{al}^d(\vec{x} - \vec{s}) K_{al}^o(\theta, \phi) u(\vec{s}, \theta, t) d\theta d\vec{s}, \tag{11}$$

where $q_r$ and $q_{al}$ are strengths of repulsion and alignment, respectively.

**Reorientation term $T(\vec{x}, \phi', \phi)$.** The reorientation term $T(\vec{x}, \phi', \phi)$ describes the rate at which an individual located at $\vec{x}$ reorients itself from $\phi'$ to $\phi$ due to influences of its neighbours — see Figure 3(a). Similar to $\lambda$, this term also takes contributions from attraction, repulsion and alignment interactions:

$$T(\vec{x}, \phi', \phi) = T_a(\vec{x}, \phi', \phi) + T_r(\vec{x}, \phi', \phi) + T_{al}(\vec{x}, \phi', \phi). \tag{12}$$

The contribution from attraction is taken to be:

$$T_a(\vec{x}, \phi', \phi) = q_a \int_{\mathbb{R}^2} \int_{-\pi}^{\pi} K_a^d(\vec{x} - \vec{s}) K_a^o(\vec{s}; \vec{x}, \phi') w_a(\phi' - \phi, \phi' - \psi) u(\vec{s}, \theta, t) d\theta d\vec{s}, \tag{13}$$

where $q_a$ and the interaction kernels are the same as before, and $w_a$ is a turning probability function that gives the probability of turning from $\phi'$ to $\phi$ due to attractive interactions with the neighbour located at $\vec{s}$.

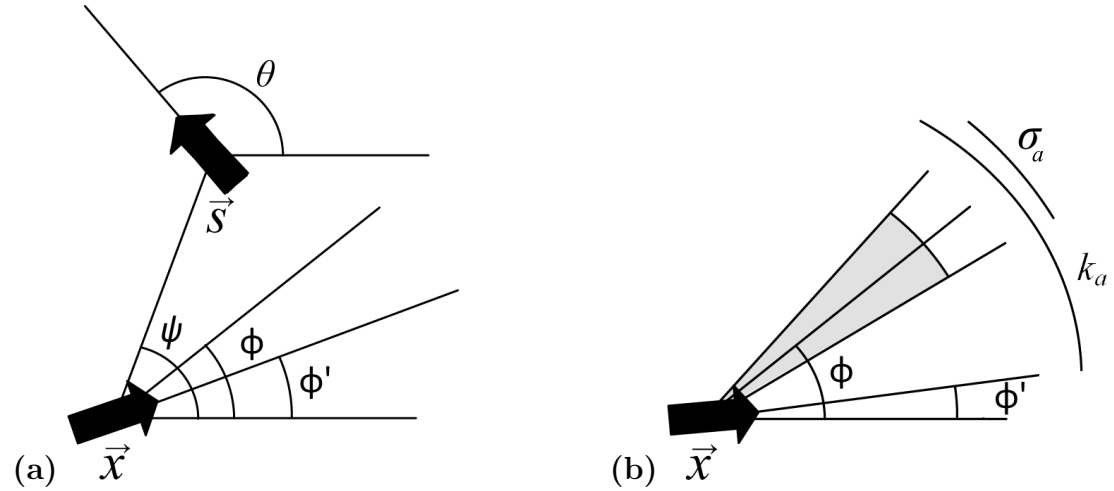


Figure 3: (a) The decision making individual at $\vec{x}$ moving in direction $\phi'$ has a probability of turning to direction $\phi$ based on its interaction with the neighbour located at $\vec{s}$ that moves in direction $\theta$. (b) Visual aide for function $g_{\sigma_a}$: the decision making individual at $\vec{x}$ moving in direction $\phi'$ has a probability to turn (due to attraction) to a direction near $\phi$, with maximum turning possibility of $k_a$ and with uncertainty $\sigma_a$.

Similarly $T_r$ and $T_{al}$ from Equation (12) are defined by

$$T_r(\vec{x},\phi',\phi) = q_r \int_{\mathbb{R}^2}\int_{-\pi}^{\pi} K_r^d(\vec{x}-\vec{s})K_r^o(\vec{s};\vec{x},\phi')w_r(\phi'-\phi,\phi'-\psi)u(\vec{s},\theta,t)d\theta d\vec{s}, \tag{14}$$

$$T_{al}(\vec{x},\phi',\phi) = q_{al} \int_{\mathbb{R}^2}\int_{-\pi}^{\pi} K_{al}^d(\vec{x}-\vec{s})K_{al}^o(\theta;\phi')w_{al}(\phi'-\phi,\phi'-\theta)u(\vec{s},\theta,t)d\theta d\vec{s}, \tag{15}$$

where $w_r$ and $w_{al}$ are probability functions which characterize the turning from direction $\phi'$ to $\phi$ due to repulsive and alignment interactions with neighbours, respectively.

Details on modelling the probability functions $w_j$ $(j = a, r, al)$ are presented in the Appendix.

Note that in the expression for $T_{al}$, the argument of $w_{al}$ includes the direction $\theta$. This is because the alignment contribution to turning does not depend on the location of the neighbours, $\psi$, but rather on their direction, $\theta$.

### 2.2 Model with a field of vision

In order to increase the biological realism of the model (1) from [1], we introduce a field of vision/ blind zone of the individuals. The model presented in Section 2.1 suggests that, in terms of attractive interactions, the neighbours behind a reference individual (see Figure 2(a)) have the strongest influence on it. However, most animals cannot see behind themselves and are not susceptible to sudden changes occurring behind them, especially when animals depend primarily on sight. We introduce here a blind zone that is in a consistent format to the model presented in Section 2.1.

The field of vision/ blind zone is modelled via an additional truncation kernel. We refer again to Figure 2(a). To correctly represent the field of vision of the reference individual $\vec{x}$, the neighbours located in front (with $\psi$ within a certain interval centred at $\phi$) should be given higher weights than

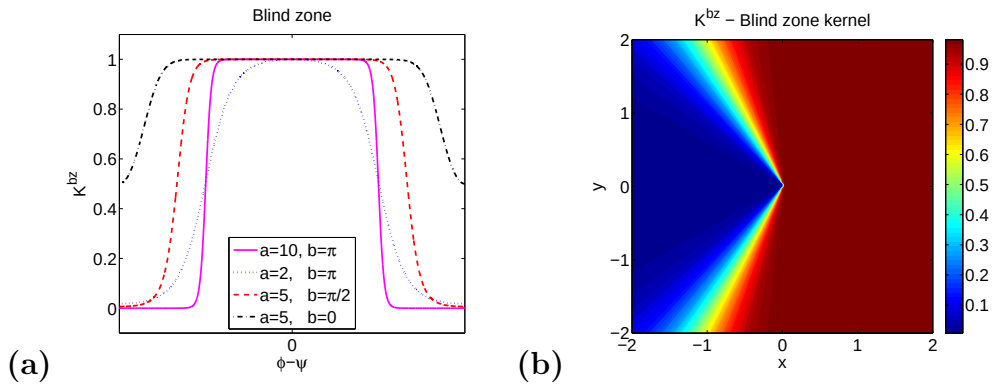


Figure 4: Field of vision. a) Plots of the function $K^{bz}$ from (16) for different values of $a$ and $b$ ($a$ controls the steepness of the graph, and $b$ its width). b) Spatial representation of $K^{bz}$ ($a = 5$, $b = \pi/2$) for a reference individual located at the origin which moves horizontally to the right. Note that $K^{bz}$ takes large and almost constant values in the direct field of vision, decays at its periphery, and has zero values in the blind zone.

the individuals located behind ($|\psi - \phi|$ close to $\pi$). We consider the following function that captures this idea:

$$K^{bz}(\phi - \psi) = \frac{1}{B}\left(\frac{1}{2}\tanh\left\{a\left[\cos(\phi - \psi) + \left(1 - \frac{b}{\pi}\right)\right]\right\} + \frac{1}{2}\right), \tag{16}$$

where $a$ and $b$ determine the *steepness* and the *width* of the field of vision, respectively, and $B$ is a constant that normalizes the kernel.

Figure 4(a) shows how changing $a$ and $b$ alters the field of vision ($a$ can range from 1 to $\infty$, and $b$ can be any real number). Note how decreasing the value of $b$ from $\pi$ to 0 increases the field of vision. A large enough *negative* value of $b$ would create a virtually flat function (plot not shown here), corresponding to a full and uniform field of vision. In Section 4 we use $b = -2\pi$ to capture a full field of vision. Alternatively, increasing $b$ up to a large enough *positive* value would shrink the field of vision to reach complete blindness. This case is not interesting biologically and it will not be studied here.

Figure 4(b) shows a spatial representation of $K^{bz}$ with $a = 5$, $b = \pi/2$ corresponding to a reference individual located at the origin which moves to the right ($\phi = 0$). The function $K^{bz}$ captures a field of vision, where it takes large and almost constant values, and a blind zone, where the function vanishes.

There are, of course, other expressions of $K^{bz}$ which capture similar behaviours. We made this specific choice for reasons related to the numerical implementation of the model. In particular, we want the kernel to be of convolution type, so that Fourier-based methods are applicable (see more details in Section 3, in particular equation (33)).

The kernel from Equation (16) is added as a *weight* to the integral definitions of the $\lambda$'s and the $T$'s from (9)-(11) and (13), (14), (15). The expressions of $\lambda_a$ and $T_a$ from (9) and (13), when a field of vision is considered, change to:

$$\lambda_a(\vec{x}, \phi) = q_a \int_{\mathbb{R}^2} \int_{-\pi}^{\pi} K_a^d(\vec{x} - \vec{s}) K^{bz}(\vec{s}; \vec{x}, \phi) K_a^o(\vec{s}; \vec{x}, \phi) u(\vec{s}, \theta, t) d\theta d\vec{s}, \tag{17}$$

$$T_a(\vec{x}, \phi', \phi) = q_a \int_{\mathbb{R}^2} \int_{-\pi}^{\pi} K_a^d(\vec{x} - \vec{s}) K^{bz}(\vec{s}; \vec{x}, \phi') K_a^o(\vec{s}; \vec{x}, \phi') w_a(\phi' - \phi, \phi' - \psi) u(\vec{s}, \theta, t) d\theta d\vec{s}. \tag{18}$$

Note that we explicitly indicated the dependence of $K^{bz}$ on $\vec{s}$, the location of the generic neighbour. The expressions for the turning rates due to repulsion and alignment change similarly.

### 2.3 Predator-prey interactions

Though biological aggregates have interesting behaviours on their own, by introducing a predator, more dynamic behaviours are observable. Predators can influence prey movement by constricting prey into tighter groups, for example dolphins [9] or minke whales [38] condensing fish into bait balls. Similarly, predators can dive through a group and split the prey, such as an Eleonora's falcon that dive bombs into a group of prey [11]. We are interested in adding a predator-prey relationship to model (1) and investigate the behaviour of the resulting model.

Consider two species: a prey of density $u^p$ and a predator (hunter) of density $u^h$. We assume that the dynamics of each species is governed by an equation of type (1), except that now interactions between members of different groups must be accounted for. In particular, prey is strongly repelled by predators and similarly, predators are strongly attracted to prey.

The model consists in the following coupled integro-differential equations for the prey and the predator:

$$\partial_t u^p + \gamma^p \vec{e}_\phi \cdot \nabla_{\vec{x}} u^p = -\lambda^p(\vec{x},\phi)u^p + \int_{-\pi}^{\pi} T^p(\vec{x},\phi',\phi)u^p(\vec{x},\phi',t)d\phi', \tag{19a}$$

$$\partial_t u^h + \gamma^h \vec{e}_\phi \cdot \nabla_{\vec{x}} u^h = -\lambda^h(\vec{x},\phi)u^h + \int_{-\pi}^{\pi} T^h(\vec{x},\phi',\phi)u^h(\vec{x},\phi',t)d\phi', \tag{19b}$$

where constants and functions with a $p$ superscript refer to the prey, while a $h$ superscript refers to the predator (hunter). The prey and predator densities advect with constant speeds $\gamma^p$ and $\gamma^h$, respectively. The modelling assumptions for the turning rates $\lambda$ and $T$ that correspond to prey and predator, are laid out below.

**Prey responds to itself and to predator.** Prey individuals interact with themselves according to the rules described in Section 2.1 (attraction, repulsion, alignment) and in addition, they try to avoid the predators. The turning rates $\lambda^p$ and $T^p$ from (19a) take contributions from all these interactions and their expressions read (compare to (8) and (12)):

$$\lambda^p(\vec{x},\phi) = \lambda^p_a(\vec{x},\phi) + \lambda^p_r(\vec{x},\phi) + \lambda^p_{al}(\vec{x},\phi) + \lambda^p_{rh}(\vec{x},\phi), \tag{20}$$

$$T^p(\vec{x},\phi',\phi) = T^p_a(\vec{x},\phi',\phi) + T^p_r(\vec{x},\phi',\phi) + T^p_{al}(\vec{x},\phi',\phi) + T^p_{rh}(\vec{x},\phi',\phi). \tag{21}$$

The first three terms in each of the right-hand-sides of (20) and (21) are defined as in Section 2.2 (see (17), (18)), and describe turning due to interactions of prey individuals among *themselves*. The additional terms $\lambda^p_{rh}$ and $T^p_{rh}$ incorporate repulsion of prey from the predator (note the subscript $h$ standing for predator/hunter).

In modelling the prey-predator components $\lambda^p_{rh}$ and $T^p_{rh}$ we follow the approach used in Section 2.1 for one species interactions. This is in fact one of the merits of this model, that it does not need extra modelling considerations to include interactions between different species. Such interactions would come naturally from the same basic setup from Section 2.1. More precisely, we assume that a prey individual has a comfort zone with respect to predators, and once a predator enters this zone (within the prey's field of vision), the prey starts turning and running away from the

predator. This comfort zone can be described using a repulsive distance kernel in the form (3), but with characteristics that refer to prey-predator interactions. We denote this kernel by $K^d_{rh}$, with a subscript $h$ that indicates that the prey's repulsive distance kernel refers to the hunter (predator).

The prey-predator contributions $\lambda^p_{rh}$ and $T^p_{rh}$ are given by:

$$\lambda^p_{rh}(\vec{x},\phi) = q_{rh}\int_{\mathbb{R}^2}\int_{-\pi}^{\pi} K^d_{rh}(\vec{x}-\vec{s})K^{bz}(\vec{s};\vec{x},\phi)K^o_r(\vec{s};\vec{x},\phi)u^h(\vec{s},\theta,t)d\theta d\vec{s}, \tag{22}$$

$$T^p_{rh}(\vec{x},\phi',\phi) = q_{rh}\int_{\mathbb{R}^2}\int_{-\pi}^{\pi} K^d_{rh}(\vec{x}-\vec{s})K^{bz}(\vec{s};\vec{x},\phi')K^o_r(\vec{s};\vec{x},\phi')w_{rh}(\phi'-\phi,\phi'-\psi)u^h(\vec{s},\theta,t)d\theta d\vec{s}. \tag{23}$$

Note that the expressions above involve integration with respect to the *other* species, in this case the predator population $u^h$. Also note that the blind zone and orientation kernels $K^{bz}$ and $K^o_r$ used in (22) and (23) are exactly the *same* kernels used to describe interactions of prey with itself. This is because it is reasonable to assume that the field of vision of a prey individual is *intrinsic* (and it does not depend on what is actually perceived in there) and also, because the orientation kernels introduced in Section 2.1 capture *generic* changes in orientation (which could result from a variety of reasons, including interactions with other prey fellows or predators). Alternatively, one could consider different perception fields of prey with respect to predators and modify the blind zone kernel in (22) and (23).

We reiterate that the prey-predator repulsive distance kernel $K^d_{rh}$ is in the form of (3), but has a *different* range $d_{rh}$, width $m_{rh}$, and normalizing constant $A_{rh}$. Also, a different value $q_{rh}$ for the strength of the prey-predator repulsion was used. Typically this is significantly larger than the strength of repulsion among prey individuals. Finally, we used a different turning probability function $w_{rh}$ to indicate different turning precision and range, described by $\sigma_{rh}$ and $k_{rh}$, respectively, when turning of prey relative to a predator is considered.

**Predator responds to itself and to the prey.** The turning/ reorientation rates $\lambda^h$ and $T^h$ in the predator equation (19b) are modelled similarly. The predator interacts with itself and is attracted to prey, behaviour captured by

$$\lambda^h(\vec{x},\phi) = \lambda^h_a(\vec{x},\phi) + \lambda^h_r(\vec{x},\phi) + \lambda^h_{al}(\vec{x},\phi) + \lambda^h_{ap}(\vec{x},\phi), \tag{24}$$

$$T^h(\vec{x},\phi',\phi) = T^h_a(\vec{x},\phi',\phi) + T^h_r(\vec{x},\phi',\phi) + T^h_{al}(\vec{x},\phi',\phi) + T^h_{ap}(\vec{x},\phi',\phi). \tag{25}$$

Similar to (20) and (21), the first three terms in each right-hand-side correspond to interactions of the predator with *itself*. The terms $\lambda^h_{ap}$ and $T^h_{ap}$ correspond to the attraction of predator towards the prey (note the subscript $p$ standing for prey).

The components $\lambda^h_j$ and $T^h_j$ $(j = a, r, al)$ in (24) and (25), which regard interactions of the predator with itself, can be modelled as in Section 2.2. Below we use *overbar* to denote predator-specific quantities and characteristics. We consider distance, orientation and blind zone kernels $\bar{K}^d_j$, $\bar{K}^o_j$ and $\bar{K}^{bz}$, respectively, specific to interactions among predators, as well as interaction strengths $\bar{q}_j$ and turning functions $\bar{w}_j$ $(j = a, r, al)$. All such characteristics are modelled as in Section 2.1. The predator distance kernels $\bar{K}^d_j$, for instance, are in the form of (3), but with ranges, widths and normalizing constants which are specific to predator-predator interactions.

We illustrate below only the attraction terms $\lambda^h_a$ and $T^h_a$ from (24) and (25), the rest are similar:

$$\lambda^h_a(\vec{x},\phi) = \bar{q}_a\int_{\mathbb{R}^2}\int_{-\pi}^{\pi} \bar{K}^d_a(\vec{x}-\vec{s})\bar{K}^{bz}(\vec{s};\vec{x},\phi)\bar{K}^o_a(\vec{s};\vec{x},\phi)u^h(\vec{s},\theta,t)d\theta d\vec{s}, \tag{26}$$

$$T_a^h(\vec{x},\phi',\phi) = \bar{q}_a \int_{\mathbb{R}^2}\int_{-\pi}^{\pi} \bar{K}_a^d(\vec{x}-\vec{s})\bar{K}^{bz}(\vec{s};\vec{x},\phi)\bar{K}_a^o(\vec{s};\vec{x},\phi)\bar{w}_a(\phi'-\phi,\phi'-\psi)u^h(\vec{s},\theta,t)d\theta d\vec{s}. \quad (27)$$

Attraction of the predator toward the prey is included in the turning rates $\lambda_{ap}^h$ and $T_{ap}^h$. Predators turn to approach and chase the prey situated in their cone of vision. It is natural to assume that the attraction range of the predator with itself is different from the attraction range of the predator with respect to prey. Therefore we use a distance kernel $\bar{K}_{ap}^d$ describing attraction of the predator toward the prey that is *different* from the distance kernel $\bar{K}_a^d$ that corresponds to attraction of predators to themselves. Similarly, the strength of attraction to the prey $\bar{q}_{ap}$ and the turning function $\bar{w}_{ap}$ relative to the prey are different from $\bar{q}_a$ and $\bar{w}_a$ used in (26) and (27). We arrive at:

$$\lambda_{ap}^h(\vec{x},\phi) = \bar{q}_{ap} \int_{\mathbb{R}^2}\int_{-\pi}^{\pi} \bar{K}_{ap}^d(\vec{x}-\vec{s})\bar{K}^{bz}(\vec{s};\vec{x},\phi)\bar{K}_a^o(\vec{s};\vec{x},\phi)u^p(\vec{s},\theta,t)d\theta d\vec{s}, \quad (28)$$

$$T_{ap}^h(\vec{x},\phi',\phi) = \bar{q}_{ap} \int_{\mathbb{R}^2}\int_{-\pi}^{\pi} \bar{K}_{ap}^d(\vec{x}-\vec{s})\bar{K}^{bz}(\vec{s};\vec{x},\phi)\bar{K}_a^o(\vec{s};\vec{x},\phi)\bar{w}_{ap}(\phi'-\phi,\phi'-\psi)u^p(\vec{s},\theta,t)d\theta d\vec{s}. \quad (29)$$

**Remark.** Using very similar ideas, the model from Section 2.2 can be altered to describe various types of relationships. Two-species interacting may not be necessarily of a predator-prey type. They could, for instance, compete for the same resources, but at the same time avoid each other. Alternatively, another stationary predator could be added that might act as an obstacle. Or a food patch can be included, as an attractive region. In theory, this model could extend to any number of species that have a variety of relationships with other species. However, our numerical investigations only focus on the single predator and single prey relationship.

# 3 Numerical method

Numerics for model (19) poses serious challenges. As a kinetic model, sampling in *both* space and velocity variables is needed, which makes the integrals on the right-hand-sides very costly to compute. Quadrature methods, for instance, would require the evaluation, at *every* gridpoint, of a sum over *all* the other gridpoints, thus having a huge impact on the computational speed. A recent work [28] presents the difficulties in simulating aggregation models with pairwise interactions, and discusses about the various methods available: fast summation methods (Fast Multipole Method), compressive sampling, Monte Carlo methods. In the present research we take a separate approach and cast the space and angle integrals as *convolutions*, then use Fourier spectral methods to evaluate them relatively cheaply in Fourier space. More specifically, the convolution of a kernel $K$ with a function $u$ can be computed in Fourier space via a simple algebraic multiplication:

$$\widehat{K * u}\,(l) = \hat{K}(l)\hat{u}(l).$$

We consider a square domain $[-\frac{L}{2},\frac{L}{2}) \times [-\frac{L}{2},\frac{L}{2})$ of side length $L$ and sample it at $N^2$ points ($N$ grid points in each space direction). The spatial grid spacing is $\Delta x = \Delta y = \frac{L}{N}$. The angle dimension has $M$ points with a domain of $2\pi$ radians, which goes from $[-\pi,\pi)$, with grid spacing of $\Delta\phi = \frac{2\pi}{M}$. To update the solution in time we use the fourth order Runge-Kutta method.

The Fast Fourier Transform (FFT) has to be used with care, as it introduces a distortion of modes called aliasing. To avoid aliasing the spatial grid is extended from $N^2$ to $(\frac{3}{2}N)^2$ and the angular grid is extended from $M$ to $\frac{3}{2}M$. The $\frac{3}{2}$ is the smallest possible factor to guarantee

that dealiasing is successful and to minimize the computational time. Some functions with this spatial and angular extension are fast Fourier transformed into the Fourier space, and then have the highest third of the frequency Fourier coefficients set to zero. The calculations are carried out in the extended real and frequency domains, and then reduced back to the original size. This dealiasing process is standard as discussed in [39].

The left-hand-sides of the integro-differential equations (19a) and (19b) are computed easily. By first taking the 2D Fourier transform of the linear convective term in (19a), it becomes

$$\gamma \left(\cos\phi \, l_1 + \sin\phi \, l_2\right) \widehat{u^p}, \tag{30}$$

where $l_1$, $l_2$ are the horizontal and vertical components of the wave number, respectively. Similarly for (19b). These new algebraic forms for the left-hand-sides can now be dealt with using the integrating factor technique.

The right-hand-sides of (19a) and (19b) are the key of the matter and require much more work. They involve the calculations of the integrals representing $\lambda$ and $T$, which we now show can be cast as convolutions. Note however that a certain component of $T$ cannot be entirely represented as a convolution and in that case we resort to quadrature methods.

Inspect first the attraction component of $\lambda^p$ given by (17) with $u$ replaced by $u^p$. It is not immediately clear that the integral in (17) represents a convolution, as both the blind zone and orientation kernels $K^{bz}$ and $K^o_a$ (see (16) and (5)) are functions of $\phi - \psi$. But we can rework their expressions, by expanding the cosine and using

$$\cos\psi = \frac{s_x}{\sqrt{s_x^2 + s_y^2}}, \qquad \sin\psi = \frac{s_y}{\sqrt{s_x^2 + s_y^2}}, \tag{31}$$

where $\vec{s} - \vec{x} = (s_x, s_y)$. The orientation kernel $K^o_a$ becomes

$$K^o_a\left(\vec{s}; \vec{x}, \phi\right) = \frac{1}{2\pi}\left(-\cos\phi \frac{s_x}{\sqrt{s_x^2 + s_y^2}} - \sin\phi \frac{s_y}{\sqrt{s_x^2 + s_y^2}} + 1\right), \tag{32}$$

which is now a function of $\vec{x} - \vec{s}$. Similarly, $K^{bz}$ can be written as a function of $\vec{x} - \vec{s}$,

$$K^{bz}(\vec{s}; \vec{x}, \phi) = \frac{1}{B}\left(\frac{1}{2}\tanh\left\{a\left[\cos\phi \frac{s_x}{\sqrt{s_x^2 + s_y^2}} + \sin\phi \frac{s_y}{\sqrt{s_x^2 + s_y^2}} + \left(1 - \frac{b}{\pi}\right)\right]\right\} + \frac{1}{2}\right), \tag{33}$$

and hence, the *spatial* integration in (17) is a convolution. Regarding the integration with respect to $\theta$, note that none of the kernels in (17) depend on angle $\theta$, it is only the density $u^p$ which depends on this variable. Hence, integration with respect to $\theta$ in (17) is simply the Fourier zero-mode of $u^p$ with respect to angle. Similar considerations apply to the attraction component of $\lambda^h$, as well as the repulsion and inter-species components of both $\lambda^p$ and $\lambda^h$. Regarding the latter, note from (22) and (28) that the only difference is that integration (and hence Fourier multiplication) is done with respect to the density of the *other* species.

The alignment component $\lambda^p_{al}$ of $\lambda^p$ can be written as a convolution in *both* space and angle variables. Indeed, the distance and blind zone kernels are functions of $\vec{x} - \vec{s}$, while the orientation kernel $K^o_{al}$ is a function of $\phi - \theta$ (see (7)). As a result, calculation of $\lambda^p_{al}$ can be done via FFT

in space and angle, where the two Fourier transforms conveniently decouple. Similarly for the alignment component $\lambda^h_{al}$ of $\lambda^h$.

The calculations of the reorientation rates $T^p$ and $T^h$ are a little more involved, due to the presence of the turning probability functions. Here we make the comment which we alluded to earlier, namely, that in order to take advantage of using FFT, we model the turning functions by a sine function (see (38)). The gain brought by this choice can be seen for instance by inspecting the attraction component (18). We noted above that the distance, blind zone and attractive orientation kernels are functions of $\vec{x} - \vec{s}$. Suppose now that $\phi$ and $\phi'$ are fixed and $v_a$ is given by (38). Then, by expanding the sine and using (31), the probability function $w_a$ from (36) can be expressed as

$$\begin{aligned} w_a\left(\phi' - \phi, \phi' - \psi\right) &= g_{\sigma_a}\left(\phi' - \phi - \kappa_a\left(\sin\phi'\cos\psi - \cos\phi'\sin\psi\right)\right) \\ &= g_{\sigma_a}\left(\phi' - \phi - \kappa_a\left(\sin\phi'\frac{s_x}{s_x^2+s_y^2} - \cos\phi'\frac{s_y}{s_x^2+s_y^2}\right)\right), \end{aligned}$$

with $g_{\sigma_a}$ given by (37). Note that the outcome is a function of $\vec{x} - \vec{s}$ and therefore, the spatial integration in the right-hand-side of (18) is a convolution which can be computed in Fourier space. Integration with respect to $\theta$ reduces to calculation of the Fourier zero-mode. Similar considerations apply to the repulsion and inter-species components of $T^p$ and $T^h$.

The alignment components of the reorientation rates have to be treated separately. For convenience we drop the superscripts $p$ or $h$ for the following calculation, therefore it applies to both populations. We have (see (15) with inclusion of blind zone):

$$T_{al}(\vec{x}, \phi', \phi) = q_{al}\int_{\mathbb{R}^2} K^d_{al}(\vec{x} - \vec{s})K^{bz}(\vec{s}; \vec{x}, \phi')\int_{-\pi}^{\pi} K^o_{al}(\theta; \phi')w_{al}(\phi' - \phi, \phi' - \theta)u(\vec{s}, \theta, t)d\theta d\vec{s}. \quad (34)$$

The integral with respect to $\theta$ is *not* a convolution and we have to resort to quadrature to compute it. We use the trapezoidal rule with a double loop, to account for all angles $\phi$ and $\phi'$. This is the most computationally expensive step of the numerical algorithm and the only place where FFT was not applicable. The integral over $\vec{s}$ can still be easily calculated with two-dimensional FFT as before.

# 4 Numerical experiments

This section will showcase the versatility of the model and how it captures a large variety of predator-prey interactions. We noted in the previous section that computing the alignment component in the reorientation rates is very expensive computationally. To increase the computational speed, we have excluded the alignment terms of the predator (but kept the alignment of the prey, an important ingredient in the model). The omission of these terms lowered the computational cost by slightly less than a factor of two. The lack of predator alignment is supported in fact by several observations on hunting strategies of dolphins [9] and lions [40]. In future work we will consider alternative formulations of alignment interactions, which can be cast as convolutions. One possible solution is to model alignment using attractive-repulsive interaction mechanisms, as in [41].

For all experiments we take the size of the domain to be $L = 4$ and the speed of the prey to be $\gamma^p = 1$. The parameters defining the ranges and widths of *all* distance kernels are also set for all experiments, unless otherwise indicated: $d_r = 0$, $d_{al} = 0.4$, $d_a = 0.8$, $d_{rh} = 0$, $\bar{d}_r = 0$, $\bar{d}_a = 0.4$, $\bar{d}_{ap} = 0.4$, $m_r = m_{al} = m_a = 0.2$, $m_{rh} = 0.8$, $\bar{m}_r = 0.2$, $\bar{m}_a = 0.2$ and $\bar{m}_{ap} = 0.4$. Recall that

the overbar means that these constants refer to the predator. For example, $\bar{m}_r$ shows the width of the zone of influence for the predator being repelled by itself, while $\bar{m}_{ap}$ shows the width of the attraction zone of the predator with respect to the prey.

The parameters defining the turning uncertainties (see equation (37)) are set for both prey and predator: $\sigma_j = \bar{\sigma}_j = 0.2$ $(j = a, r, al)$. The parameters which characterize the blind zone of the prey are also fixed at $a = 10$, $b = \frac{\pi}{2}$, with the exception of the blind zone experiments, which show the effect of changing the blind zone.

All figures below plot the *spatial* (or macroscopic) population densities $\rho^p$ and $\rho^h$, defined by

$$\rho^p(\vec{x}, t) = \int_{-\pi}^{\pi} u^p(\vec{x}, \phi, t)\, d\phi \quad \text{and} \quad \rho^h(\vec{x}, t) = \int_{-\pi}^{\pi} u^h(\vec{x}, \phi, t)\, d\phi,$$

respectively. We present contour plots of these functions, with magnitudes indicated by colour bars. A small white arrow attached to a spatial location indicates the average direction an individual located at that grid point is moving in. The size of the arrows shows the relative amount of motion of the individuals.

### 4.1 Stationary predator

**Predator ring.** Predators sometimes cannot rely on speed and agility to catch their prey. Nevertheless they can come up with clever ways to catch their prey which take less effort and are more efficient. One such method is the predator ring. The predators can surround the prey, forcing it into a ball, which condenses the group. This makes a higher probability of the predator catching its prey. Figure 5 shows the predator ring in the top left figure, and five plots of the prey moving around the centre of the ring.

The parameters for this experiment are: $q_r = 4$, $q_{al} = 5$, $q_a = 1$, $q_{rh} = 20$, $k_r = -0.65$, $k_{al} = 0.85$, $k_a = 0.85$ and $k_{rh} = -0.7$. The strength of repulsion, $q_r$, is larger than the strength of attraction, $q_a$, which would cause the prey to disperse in the absence of the predator. The value of $q_{rh}$, the strength of prey-predator repulsion, is large, which forces the prey to keep a large distance from the predator. The zonal width $m_{rh}$ was changed from 0.8 to 0.6 in this experiment to allow the prey to be closer to the predator ring, instead of having it confined to the centre of the ring. The prey's initial condition is a small counter-clockwise rotating ball which eventually spreads apart. Because of this initial condition, the prey deflects off of the predator ring and continues in its counter-clockwise fashion.

The behaviour of a predator ring is common in nature in a variety of forms. One such form is that of dolphins, which execute herding passes to condense fish into bait balls [9]. Cooperative hunting by surrounding the prey has also been seen in lions [40]. Confining prey in this way makes it more efficient for the predator to capture it.

### 4.2 Moving predator (no turning)

Even though it is important that the prey behave realistically around a stationary predator, much more happens when the predator is in motion. A moving predator can cause the prey to turn as a group, split or disperse. Since the predator can now come up behind the prey, the blind zone of the prey plays a large role in how the group behaves. Also this section is used as a building block for when the predator is also allowed to turn (see Section 4.3).

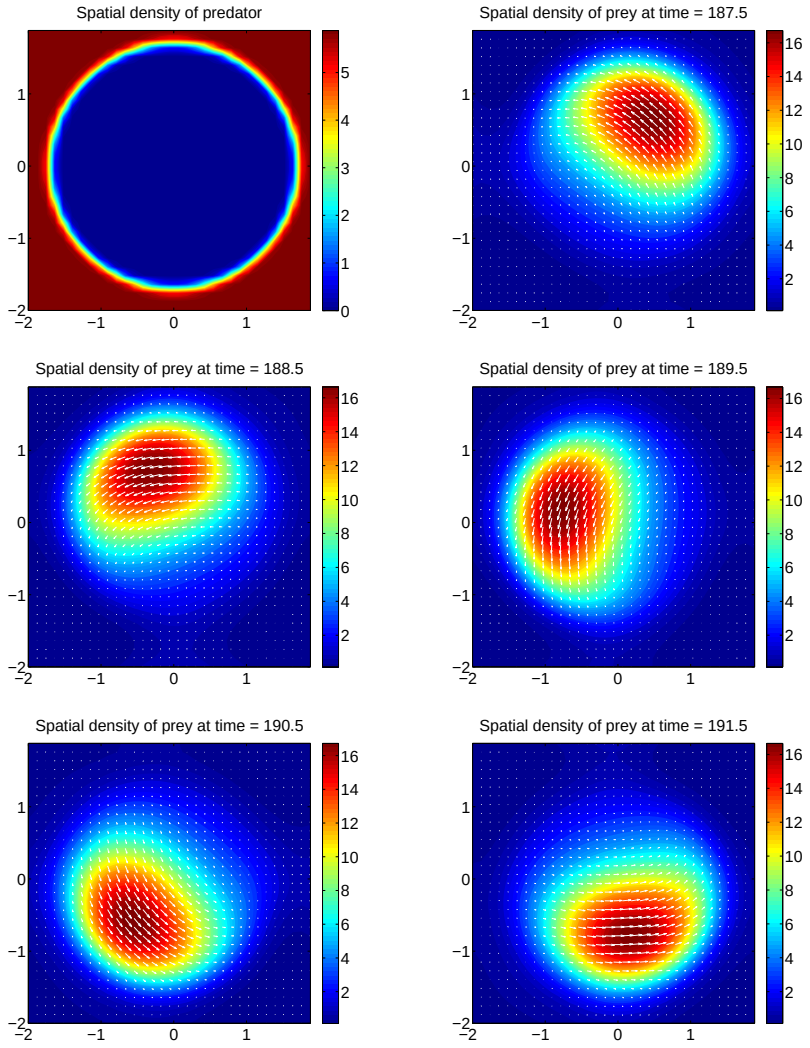


Figure 5: Predator ring: A sequence showing the prey enclosed by a predator ring. The top left plot is the predator and the other five are the prey. The prey move in a circle, continually trying to avoid the predator, but the prey are trapped.

**a. Prey moving towards the predator.** In this experiment the initial condition is set up for the prey and predator to collide head on. To keep the experiment simple, the predator is a perfect Gaussian bump that is moved to the left as time progresses with speed $\gamma^h = 1.2$. This means the predator will not change its direction or shape. As the predator moves towards a group of prey, which is also moving towards the predator, the prey behave differently based on the two parameters of $q_a$ and $q_{al}$. The other parameters for this experiment are set at: $q_r = 1$, $q_{rh} = 40$, $k_r = -0.4$, $k_{al} = 0.8$, $k_a = 0.8$, and $k_{rh} = -0.95$.

Figure 6 shows this experiment with the plots occurring sequentially from left to right. The top row is the predator, the rest of the rows are the prey. The second row has $q_a = 1$ and $q_{al} = 1$ and shows a splitting, followed by dispersion of the group. The third row is a different simulation, with $q_a = 1$ and $q_{al} = 5$, that shows a more biased splitting of the group. Since alignment is larger, the prey will decide to turn the same way as the majority even if that puts them in harms reach of the predator. The last row is also a different simulation having $q_a = 5$ and $q_{al} = 1$, and shows the group turning around and staying together. Since the attraction is large, the prey tries hard not to split and actually does a complete turn to avoid the predator. Eventually the prey will fan out and then split from the constant pursuit of the predator.

This experiment shows a variety of behaviours this model can produce with only changing a few parameters. It mimics a lunging predator and the prey must perform an evasive tactic to escape from the predator [42].

**b. Away from predator - blind zone - alignment.** This experiment is designed to observe how the blind zone factor effects the behaviour of the prey. The initial condition has both the prey and predator moving to the left. Depending on the size of its blind zone, the prey will have more or less information to make a decision to turn to avoid the chasing predator. The essential parameter in this study is the width of the field of vision, measured by $b$ (see Figure 4(a)). We set the steepness of the peripheral vision at $a = 10$, and we vary only the values of $b$, while keeping the other parameters fixed at the following values: $\gamma^h = 1.2$, $q_r = 1$, $q_{al} = 5$, $q_a = 1$, $q_{rh} = 40$, $k_r = -0.4$, $k_{al} = 0.8$, $k_a = 0.8$ and $k_{rh} = -0.95$. Note that alignment dominates the social interactions among prey ($q_{al} > q_r$ and $q_{al} > q_a$).

In Figure 7 the top row is the predator and all the other plots show the prey. The plots occur sequentially from left to right. The second row has $b = -2\pi$ (full field of vision, no blind zone) and shows a biased splitting of the group. We remind the reader that a sufficiently large *negative* value of $b$ is needed to ensure that there is no contribution from the blind zone factor. The third row has $b = \pi/2$ and shows a less biased splitting of the group. There are more individuals moving down compared to the $b = -2\pi$ case. The last row has a larger blind zone with $b = \pi$ (see Figure 4(a)) and shows an even less biased splitting of the group. The only reason this case does not split perfectly into two equal size groups is because the initial conditions were not symmetric. Also the strong alignment will exaggerate the splitting by bringing more individuals from the group with less to the group with more.

The increase of the blind zone causes the group to split more. The value of the width of the blind zone plays a significant role in the behaviour of the prey. Another test of the effects of the blind zone was done in [26], where a milling group turned into a carousel group and then to a freely moving group by increasing the blind zone.

**Remark.** The experiments shown on the second and third rows in Figure 6 and those in Figure 7 capture two essential strategies used by prey to escape the predator: *group splitting* and *dispersal*.

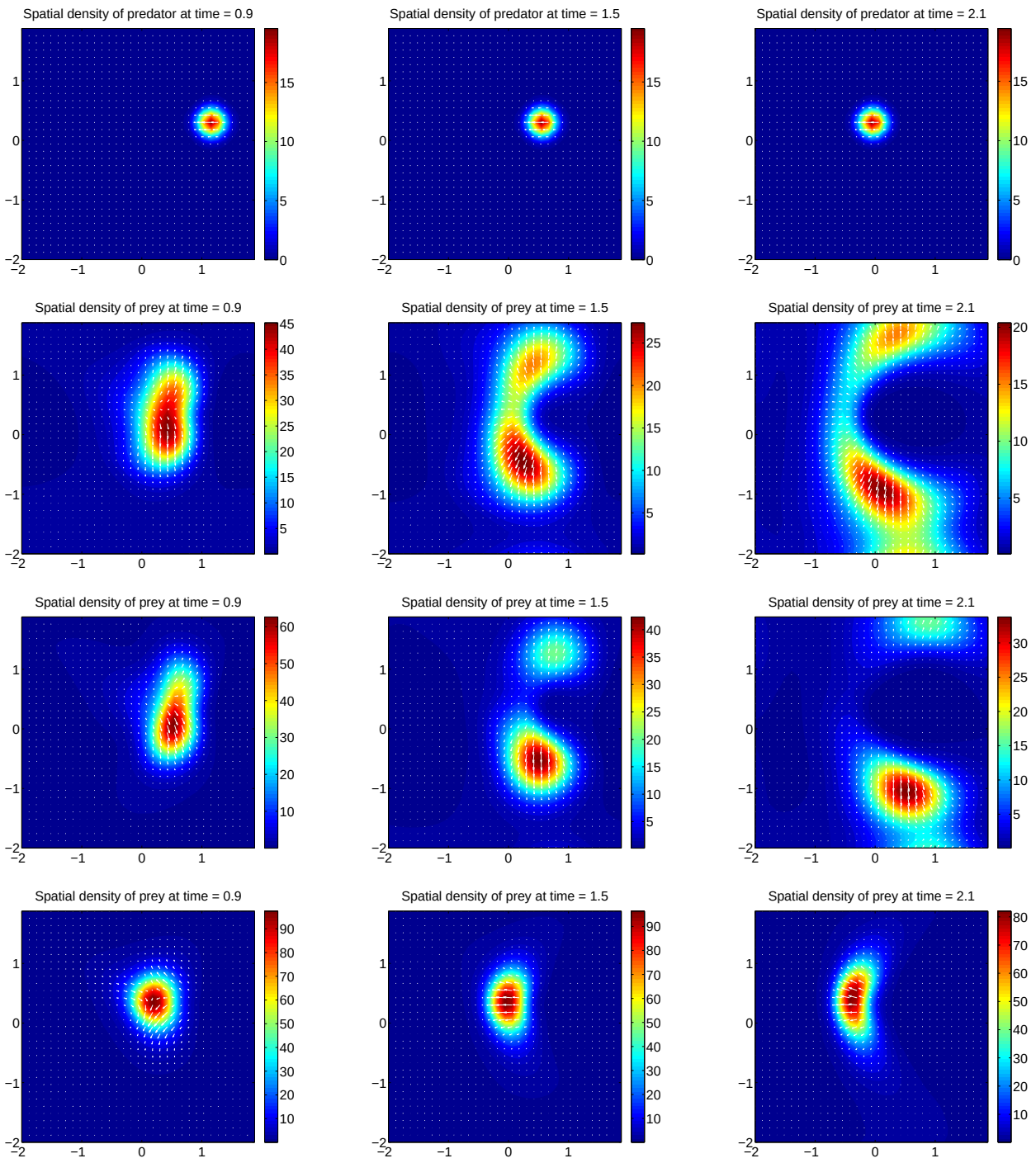


Figure 6: Prey moving towards the predator: The plots occur from left to right. The top row is the predator, the rest of the rows are the prey. The second row has $q_a = 1$ and $q_{al} = 1$ and shows the group splitting. A more biased splitting of the group occurs in the third row which has $q_a = 1$ and $q_{al} = 5$. The last row has $q_a = 5$ and $q_{al} = 1$ and shows the group turning completely around.

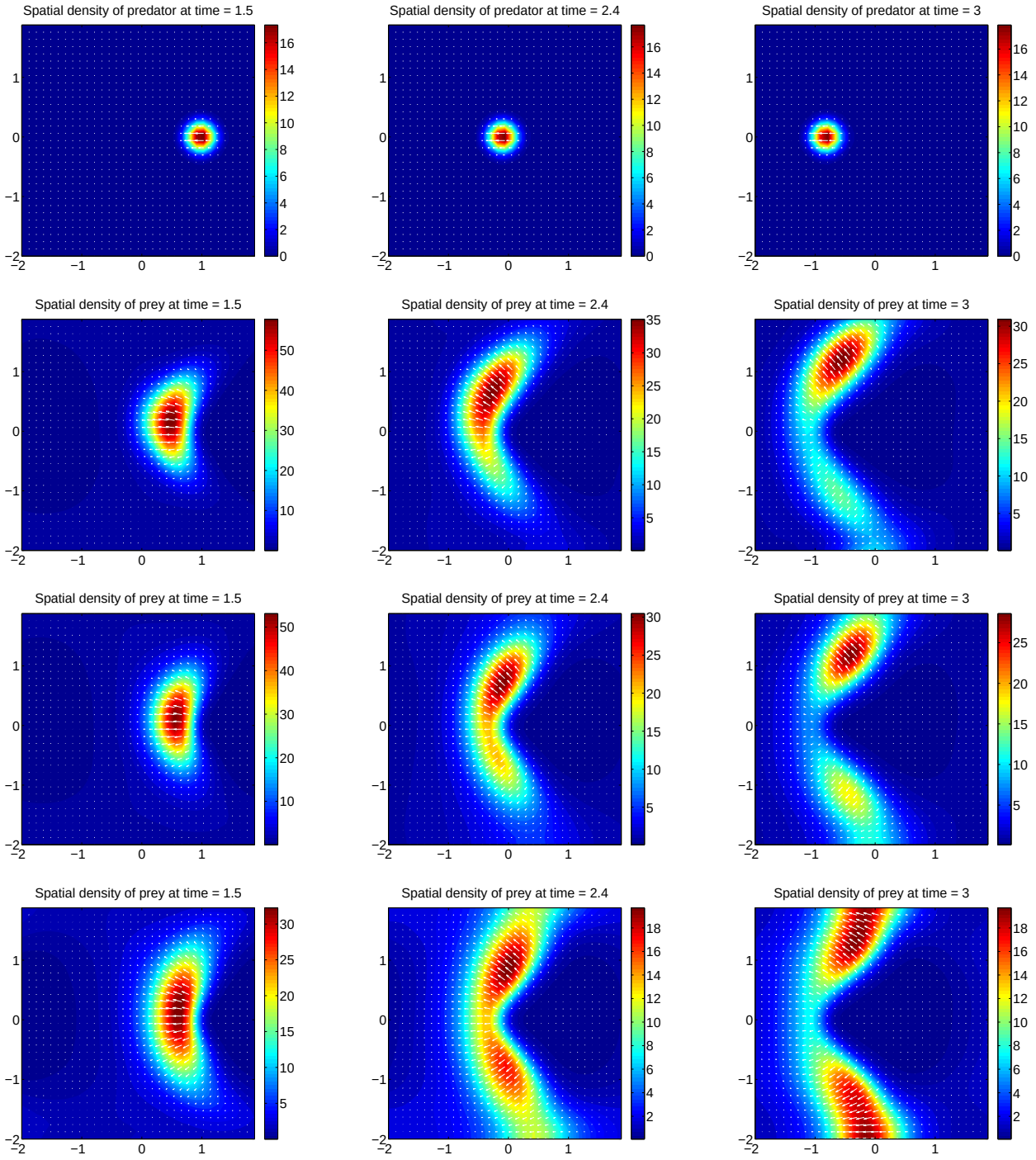


Figure 7: Away from predator - blind zone - alignment: The predator is set to chase the prey from inside the prey's blind zone. The plots occur sequentially from left to right. The top row is the predator, while the next three rows are the prey with increasingly large blind zone: $b$ equal to $-2\pi$ (no blind zone), $\frac{\pi}{2}$ and $\pi$, respectively. Since the strength of alignment, $q_{al} = 5$, is much larger than the strength of repulsion and attraction, $q_r = 1$ and $q_a = 1$ respectively, the prey's main concerns are to avoid the predator and to align with the group.

When the predators are too close, the repulsion from the predators on the prey is too great for the group to stay together. As a result, some of the prey will move away from the group in order to save themselves, ignoring any group cohesiveness. Because the predator follows the largest density, the individuals that break off from the group have a higher likelihood of not being caught. Dispersal of prey would help minimize casualties in the case of wolves attacking sheep for instance. The dispersing behaviour is common in fish (the so called "flash expansion"), as discussed in [42, 43].

**c. Away from predator - blind zone - attraction.** This experiment is another example of how the blind zone plays a role in the behaviour of the prey. The parameters and initial conditions are identical to the ones in the previous experiment, with exception of $q_a$ and $q_{al}$, which are now equal to 5 and 1 respectively.

The plots in Figure 8 occur sequentially from left to right. The top row is the predator, the rest are the prey. The second row has $b = -2\pi$ (no blind zone) and shows a high density group turning together to avoid the predator. The third row has a blind zone width $b = \pi/2$ and shows a greater amount of turning. The last row has $b = \pi$ and shows less density and a slight separation of individuals from the group. Since the strength of attraction, $q_a = 5$, is larger than the strengths of repulsion and alignment, one would think the group would remain together, but this does not happen. When the prey have a blind zone of $\pi$, there is not as much information that is passed around the individuals in comparison to the zero blind zone case. A larger field of vision enabled the prey to stay together more. Depending on the type of predator and prey, this behaviour may be advantageous or disadvantageous.

More interesting than the $b = \pi$ case is the $b = \frac{\pi}{2}$ case. Looking at the small arrows inside the spatial density of the prey at time 2.4 for the $b = \frac{\pi}{2}$ case, one can see that the individuals are moving up to the right. In the other two cases, the individuals are moving more up than right. Some fish will swim in a circle and arrive back at their starting point when a lunging predator comes by, an evasion tactic called fountain [42, 44]. This behaviour was not captured, due to complications with the periodic boundary conditions, but the case with $b = \frac{\pi}{2}$ shows some promise that this behaviour can be captured. One can imagine that if the predator is to continue moving to the left, if the boundary conditions are nonexistent and if there are two symmetric groups that avoided the predator, then these two groups would be attracted together and eventually reform the original group.

The tight turning behaviour shown in Figure 8 is seen in the prey species of the Eleonora's falcon [11]. One tactic prey can use to avoid a predator is to initiate tight turns at high speed. Since the Eleonora's falcon is larger than its prey, the prey have a higher chance of escape when using this tactic.

### 4.3 Moving predator (with turning)

While a predetermined behaviour of a predator can capture small moments of believable reactions of prey, a turning predator is much more realistic. We assume now that the predator reacts to the prey and equations (24) and (25) are implemented for all remaining experiments. Since the predator is no longer of a fixed shape, it is better to think of the predator as a group of predators. In these experiments we assign a field of vision to the predators as well. The blind zone parameters of the predators are fixed at $a = 10$, $b = \frac{\pi}{2}$.

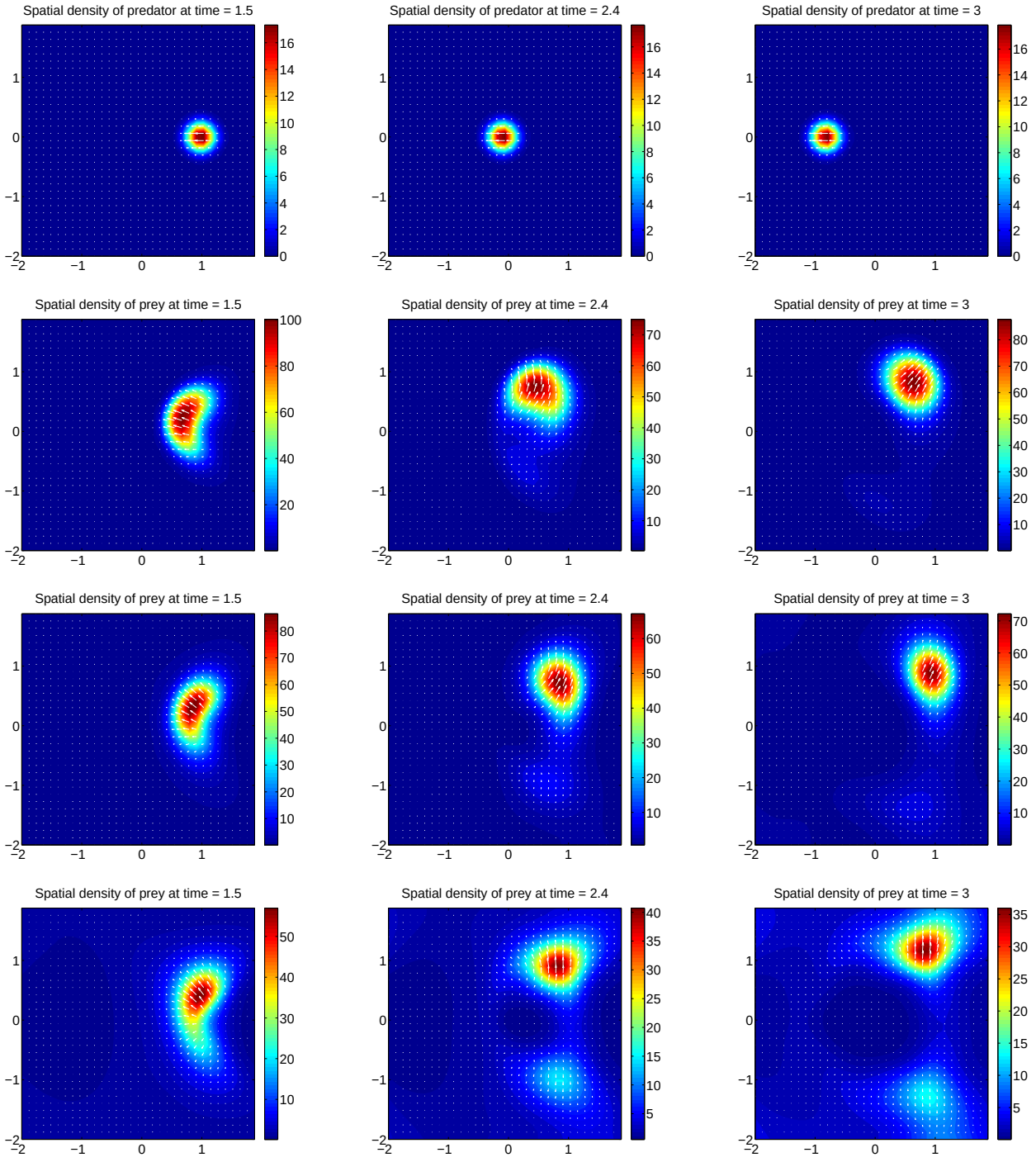


Figure 8: Away from predator - blind zone - attraction: The predator is set to chase the prey from inside the prey's blind zone. The plots occur sequentially from left to right. The top row is the predator, while the next three rows are the prey with increasingly large blind zone width: $b$ equal to $-2\pi$ (no blind zone), $\frac{\pi}{2}$ and $\pi$, respectively. Since the strength of attraction, $q_a = 5$, is much larger than the strength of repulsion and alignment, $q_r = 1$ and $q_{al} = 1$ respectively, the prey's main concerns are to avoid the predator and to stay together.

**a. Fast predator.** In this experiment the predators' speed is increased from $\gamma^h = 1.0$ to $\gamma^h = 1.5$. The predator can now move faster than the prey. The other parameters are: $q_r = 2$, $q_{al} = 5$, $q_a = 5$, $q_{rh} = 8$, $\bar{q}_r = 8$, $\bar{q}_a = 16$, $\bar{q}_{ap} = 6$, $k_r = -0.6$, $k_{al} = 0.6$, $k_a = 0.6$, $k_{rh} = -0.95$, $\bar{k}_r = -0.6$, $\bar{k}_a = 0.6$ and $\bar{k}_{ap} = 0.95$. A steady state is reached where the predators occupy the same location as the prey and they both move in the same direction with the same speed. The predators are exploiting the slowness of the prey and it can be thought of as the predators having a feast on the prey (see Figure 9). The plots on the left of Figure 9 show the prey, while the right plots show the predators. The top row shows the initial conditions, which has the predators and the prey colliding head on. The next two rows show later times with the middle row being time 10 and the bottom row being at time 25. This shows how the prey and predator move up to the left and do not change form, hence making this a translational steady state. Note that the prey and predator traverse the domain twice from time 10 to time 25.

In nature predators are not often 50% faster than their prey. In this case the predators would eat all of the prey and the prey would not have a chance to evolve to be faster. However, this speed discrepancy is common when fish are in their juvenile stages. Often slow individuals will find places to hide or use other defences. Moving fast for a predator is a huge advantage in capturing prey. The tuna and the lamnid shark have evolved to have counter-current heat-exchange mechanisms for conserving metabolic heat and raising their body temperatures [45]. These warmer muscles give extra power and create faster swimming. Most predators would benefit from having a faster movement speed.

**b. Slow predator.** In this experiment the predators' speed is reduced from $\gamma^h = 1$ to $\gamma^h = 0.25$. The initial condition for this experiment is the predators and the prey both being groups that are not directed toward each other as seen in the first row of Figure 10. The rest of the rows in Figure 10 show three progressive steps in time for the prey in the left column and the predators in the right column. The prey, though much faster than the predators, get trapped between the predators and move in a circular motion. The predators disperse and once they become close enough, they make their attempt at the prey. The parameters for this experiment are: $q_r = 2$, $q_{al} = 5$, $q_a = 5$, $q_{rh} = 20$, $\bar{q}_r = 20$, $\bar{q}_a = 0$, $\bar{q}_{ap} = 0.1$, $k_r = -0.6$, $k_{al} = 0.6$, $k_a = 0.6$, $k_{rh} = -0.8$, $\bar{k}_r = -0.6$, $\bar{k}_a = 0.6$ and $\bar{k}_{ap} = 0.6$.

It has been observed that slow predators use special hunting techniques or strategies to capture the prey. One technique is that of the frogfish, a slow predator that uses a very fast capture technique. It waits for its prey to approach and then uses enormous suction pressure to engulf its prey [46]. Similar hunting techniques have also been noted in pikes [44]. The experiment shown in Figure 10 relates to the group chase simulated in [47], where predators disperse and surround the prey.

**c. Double predator split.** This experiment shows how the predators can be clever about how they catch prey. The initial condition is a random distribution in space and angle. The parameters for this experiment are: $\gamma^h = 2$, $q_r = 1.8676$, $q_{al} = 4.3989$, $q_a = 5.9724$, $q_{rh} = 50$, $\bar{q}_r = 8$, $\bar{q}_a = 10$, $\bar{q}_{ap} = 24$, $k_r = -0.6$, $k_{al} = 0.6$, $k_a = 0.6$, $k_{rh} = -0.95$, $\bar{k}_r = -0.5$, $\bar{k}_a = 0.8$ and $\bar{k}_{ap} = 0.95$. These parameters allow the predators and the prey to stay as a group or allow them to split quickly if need be. Figure 11 shows a sequence of two predator groups working together to split the prey. The left column is the prey while the right column is the predators. The top row shows the predators splitting to follow the two separate groups of prey. The middle two plots show the two predator

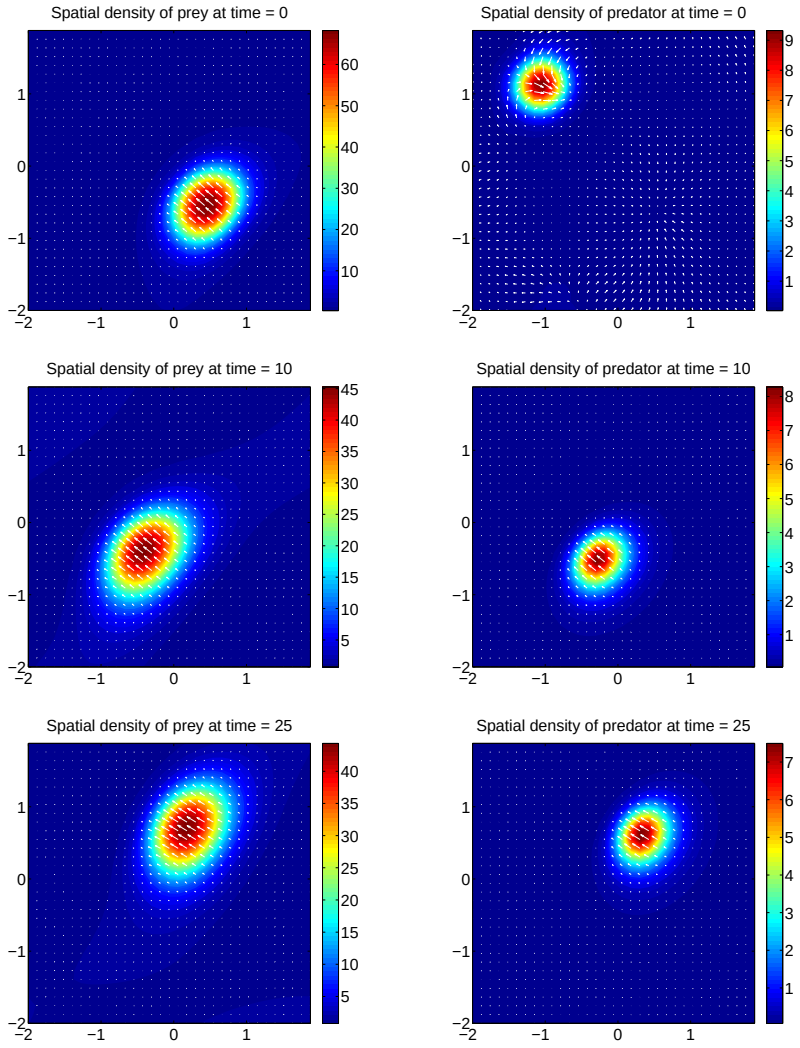


Figure 9: Fast predators: The prey are shown in the left column, while the predators are shown in the right column. Fast predators, with speed $\gamma^h = 1.5$, can catch up and keep up with their prey. This translational steady state shows the predators feasting.

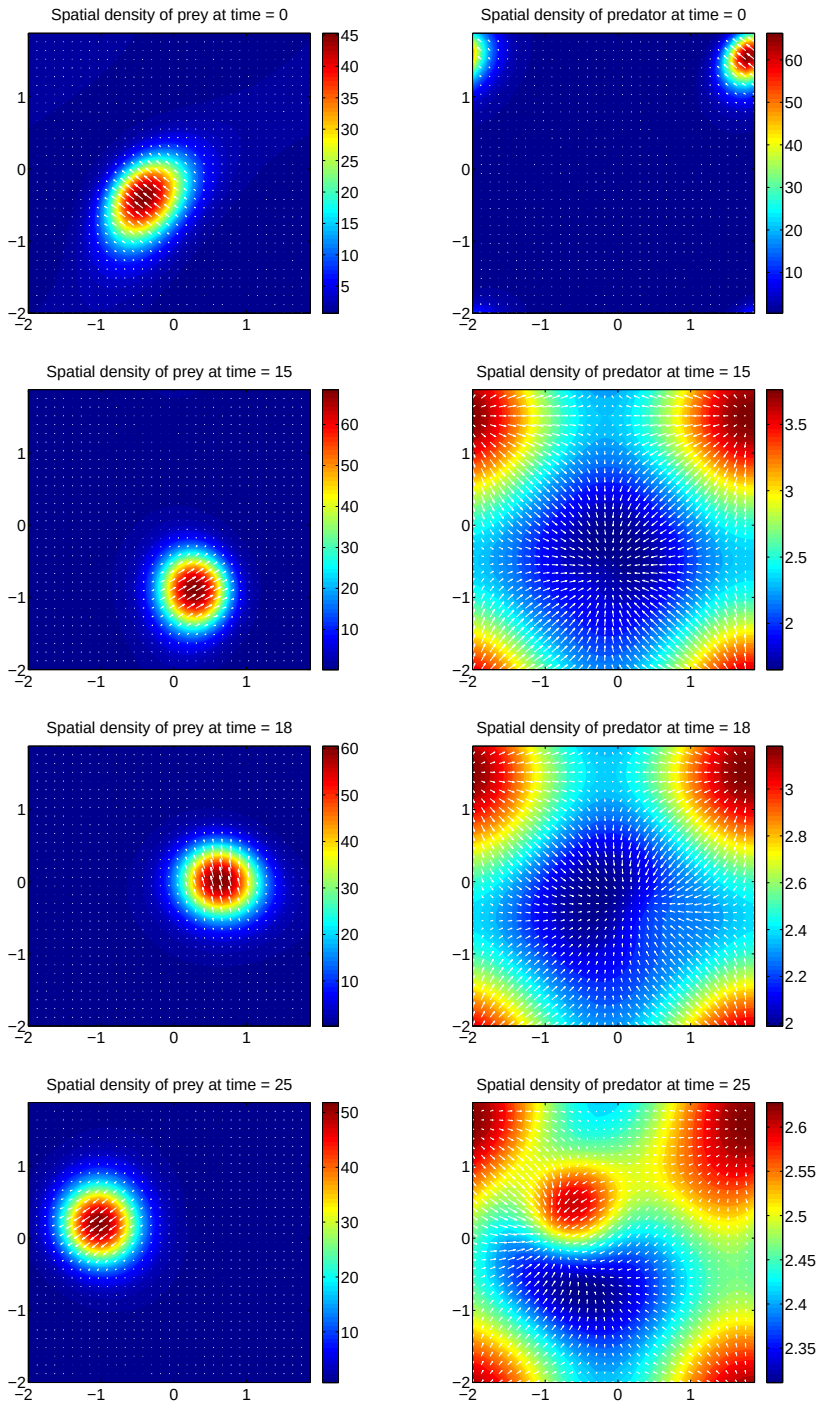


Figure 10: Slow predators: The prey are shown in the left column, while the predators are shown in the right column. Slow predators, with speed $\gamma^h = 0.25$, spread and surround their prey. The prey become trapped and move in a circular motion. At time 25 the predator forms a higher density group to feast on the prey.

groups trapping the prey. The bottom row shows the prey escaping from both predator groups by moving up or down and the predator groups collide. After the prey splits up and down they merge again and then split left and right, which brings them back to the position in the first plot (See Figure 11). This is a reoccurring pattern and there are likely many more to discover using this model.

The wild dog shows elaborate hunting techniques. They have one of the highest capture rates for a predator in the savanna [48]. Their techniques emphasize stamina instead of speed. Their ability to work as a group is also advantageous. Group members take turns chasing the prey, while trailing predators can cut corners, and eventually the prey, such as young, old or sick, will tire and be captured [48]. The ability for the predator group to split and work as a team is showcased in Figure 11. All of the complexities of the wild dogs' hunting techniques are not demonstrated here, however this model showcases a team effort by predators.

# 5 Discussion and concluding remarks

We demonstrated that our model generates realistic qualitative results that can be related to specific examples of predator-prey behaviour in nature [49, 50]. Our focus in this paper was to illustrate the hunting/escape strategies and for this reason we ignored the birth/death processes, including the feasting of predator on the prey. Such processes will be considered in future work. We showed that depending on the size of its field of vision, a prey's escape may have different outcomes. Also, it is important in an escape what interactions are dominant among the prey individuals, as the prey may split (and disperse) or stay together. Some prey species, such as those of Eleonora's falcons [11], prefer tight turns (Figure 8), others, such as minnows [44], disperse (Figure 7). On the other hand, predators develop their own hunting strategies, such as dolphins confining the prey [9] (Figure 5) or wild dogs splitting to chase and tire out the prey [48] (Figure 11).

The grouping behaviour of animals has advantages and disadvantages. A clear advantage is protection. In the presence of a predator, an animal in a group has a higher chance of survival, as there are more potential prey for the predator to catch. When trying to escape a predator, the risk of being caught is reduced if the prey individual places itself between another prey individual and the predator (selfish herd model [51]). All prey groups from Figures 5-11 have larger densities in the centre, illustrating this concept. Another instance of protection is when a school of fish confuses a predator by appearing large and making it difficult for the predator to focus on only one fish [9] (flash expansions in Figure 7). Also related, the larger a school of fish is, the more predators are required to constrict the fish into a bait ball for easier capture [9]. One disadvantage of being in a group is there may not be enough food for everyone when the group is foraging. Another disadvantage is an increase of predation because a large group is hard to hide. Despite the fact that finding a group takes a predator more time, a large group is still more conspicuous than an individual.

The predator is governed by the same basic moving principles as the prey, movement at constant speed and turning. Hence, the predator's density satisfies an equation similar to that of the prey, making the model cohesive. One can replicate the process by including any desired number of predators or prey, or any combination of interacting species. Food patches or undesired locations/obstacles can be introduced too by making certain locations attractive or repellant, respectively. By including a second group of predators (which could be of the same type as the first, but performing different hunting approaches), the model can incorporate group capture techniques

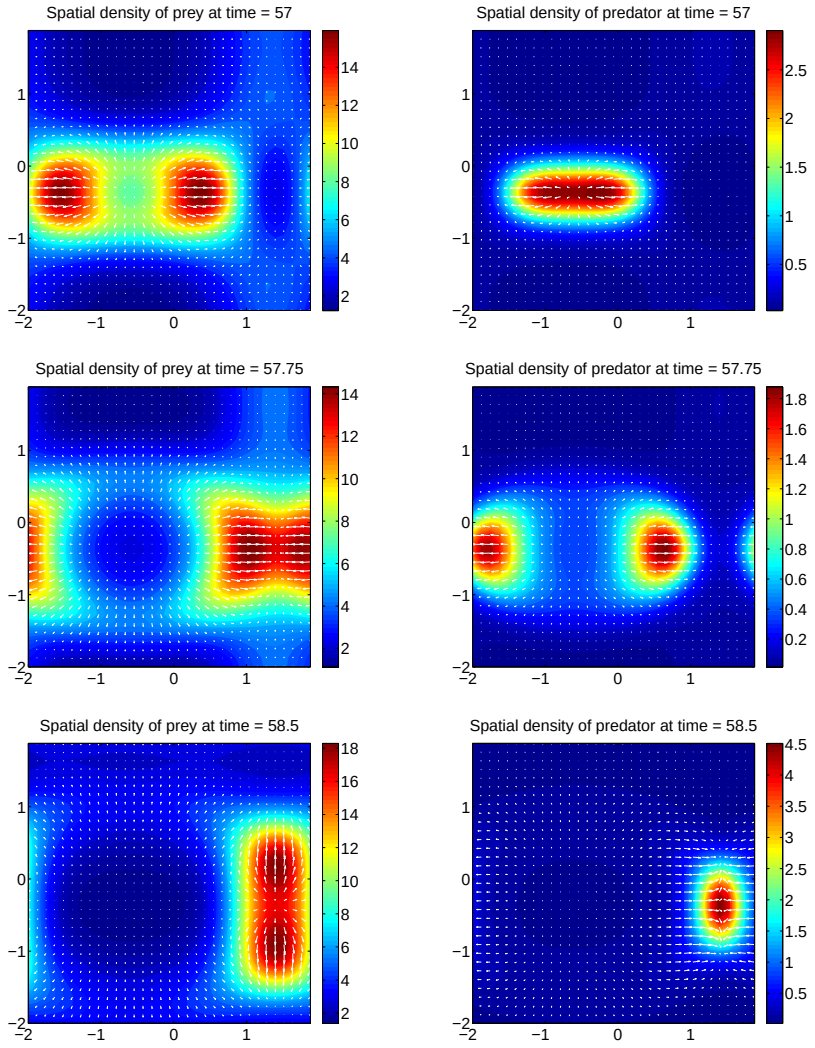


Figure 11: Double predator split: The prey are shown in the left column, while the predators are shown in the right column. The predators work as a team when chasing the prey. The predators come toward the group of prey from two angles and force the prey to split.

and strategies that increase the efficiency of the hunt. The list of possible future directions regarding this work does not stop here. Birth and death terms would have to be considered, to investigate the long time behaviour of the predator-prey dynamics. Implementing other numerical methods, such as Monte Carlo methods [28], would potentially make the numerics faster, and also, remove the periodic boundary conditions. Finally, an extension of the model to three dimensions would be very interesting to study.

# 6 Appendix

**Modelling the probability functions in equations** (13)-(15)**.** We first describe the modelling of $w_a$. Since $w_a$ is a probability function, we have

$$\int_{-\pi}^{\pi} w_a\left(\phi' - \phi, \phi' - \psi\right) d\phi = 1. \tag{35}$$

The probability function $w_a$ is modelled by

$$w_a\left(\phi' - \phi, \phi' - \psi\right) = g_{\sigma_a}\left(\phi' - \phi - v_a\left(\phi' - \psi\right)\right), \tag{36}$$

where $g_{\sigma_a}$ is an approximation of the delta function with width $\sigma_a$, and $v_a$ is a *turning function*. The decision making individual can turn to any direction within a specific range. This range is centred around direction

$$\phi = \phi' - v_a\left(\phi' - \psi\right),$$

which is when the argument of the function $g_{\sigma_a}$ is zero. The parameter $\sigma_a > 0$ measures the width of the turning range the decision making individual will move into — see Figure 3(b). The smaller the $\sigma_a$, the more accurate the turning. If $\sigma_a$ is large, then the range is wide and the decision making individual can move anywhere within the range.

The function to describe $g_{\sigma_a}$ is taken to be

$$g_{\sigma_a}(\eta) = \frac{1}{\sqrt{\pi}\sigma_a} \sum_{z\in\mathbb{Z}} e^{-\left(\frac{\eta+2\pi z}{\sigma_a}\right)^2}, \tag{37}$$

which is a periodic Gaussian with extra contributions from full rotations.

The turning function $v_a$ is modelled as

$$v_a(\eta) = k_a \sin\eta, \tag{38}$$

where $k_a$ is a constant between 0 and 1 that describes how much the decision making individual will turn due to attraction (see Figure 3(b)).

An alternative choice is $v_a(\eta) = k_a\eta$, which may be more biologically realistic. However the choice (38) for $v_a$ is made because it is periodic and works well with the fast Fourier transform, which the numerics in this paper is based on, as discussed in Section 3.

The probability functions $w_r$ and $w_{al}$ are defined through the same steps as equations (36)-(38), using approximations $g_{\sigma_r}$, $g_{\sigma_{al}}$ to the delta function, with widths $\sigma_r$, $\sigma_{al}$, turning functions $v_r$, $v_{al}$, and turning strengths $k_r$, $k_{al}$, respectively.

There is a major difference between $w_a$ and $w_r$ which has to be pointed out. Namely, in the definition of $w_r$, $k_r$ must be between $-1$ and 0 instead of between 0 and 1, as is $k_a$. This is the

only place where the negative factor comes in to enforce the negative behaviour of the repulsion interaction. The attraction and alignment interactions are positive because they respond positively to the surrounding individuals.

**Acknowledgements** R.F. was supported by NSERC Discovery Grant PIN-341834. Both R.F. and J.M. want to thank John Stockie for various suggestions and stimulating discussions during this research.

## References

[1] R. Fetecau, Collective behaviour of biological aggregations in two dimensions: a nonlocal kinetic model, Math. Mod. Meth. Appl. S. (M3AS) 21 (7) (2011) 1539–1569.

[2] T. Feder, Statistical physics is for the birds, Physics Today 60 (10) (2007) 28–30.

[3] B. Uvarov, Grasshoppers and locusts, Centre for Overseas Pest Research, London, 1966.

[4] J. K. Parrish, L. E. Keshet, Complexity, pattern, and evolutionary trade-offs in animal aggregation, Science 284 (1999) 99–101.

[5] A. B. T. Barbaro, K. Taylor, P. F. Trethewey, L. Youseff, B. Birnir, Discrete and continuous models of the dynamics of pelagic fish: application to the capelin, Math. Comput. Simulation 79 (12) (2009) 3397–3414.

[6] T. Balch, R. C. Arkin, Behavior-based formation control for multi-robot teams, IEEE Transactions on Robotics and Automation 14 (6) (1998) 926–939.

[7] D. J. Cook, P. Gmytrasiewicz, L. B. Holder, Decision-theoretic cooperative sensor planning, IEEE Transactions on Pattern Analysis and Machine Intelligence 18 (10) (1996) 1013–1023.

[8] G. Naldi, L. Pareschi, G. Toscani (Eds.), Mathematical Modeling of Collective Behavior in Socio-Economic and Life Sciences, Modeling and Simulation in Science, Engineering and Technology, Birkhäuser, New York, 2010.

[9] R. L. Vaughn, E. Muzi, J. Richardson, B. Würsig, Dolphin bait-balling behaviors in relation to prey ball escape behaviors, J. Ethology 117 (2011) 859–871.

[10] K. A. J. White, J. D. Murray, M. A. Lewis, Wolf-deer interactions: a mathematical model, Proc. R.Soc. Lond. B 263 (1996) 299–305.

[11] A. Hedenström, M. Rosén, Predator versus prey: on aerial hunting and escape strategies in birds, Int. Soc. Behav. Ecology 12 (2) (2001) 150–156.

[12] I. D. Couzin, J. Krause, R. James, G. Ruxton, N. R. Franks, Collective memory and spatial sorting in animal groups, J. Theor. Biol. 218 (2002) 1–11.

[13] F. Cucker, S. Smale, Emergent behavior in flocks, IEEE Trans. Automat. Control 52 (5) (2007) 852–862.

[14] M. R. D'Orsogna, Y.-L. Chuang, A. L. Bertozzi, L. S. Chayes, Self-propelled particles with soft-core interactions: patterns, stability and collapse, Phys. Rev. Lett. 96 (10) (2006) 104302.

[15] S.-Y. Ha, E. Tadmor, From particle to kinetic and hydrodynamic descriptions of flocking, Kinet. Relat. Models 1 (3) (2008) 415–435.

[16] J. A. Carrillo, M. Fornasier, G. Toscani, F. Vecil, Particle, kinetic, and hydrodynamic models of swarming, in: G. Naldi, L. Pareschi, G. Toscani (Eds.), Mathematical Modeling of Collective Behavior in Socio-Economic and Life Sciences, Birkhäuser, New York, 2010, pp. 297–336.

[17] E. Bertin, M. Droz, G. Grégoire, Hydrodynamic equations for self-propelled particles: microscopic derivation and stability analysis, J. Phys. A: Math. Theor. 42 (2009) 445001.

[18] H. G. Othmer, S. R. Dunbar, W. Alt, Models of dispersal in biological systems, J. Math. Biol 26 (1988) 263–298.

[19] A. Mogilner, L. Edelstein-Keshet, A non-local model for a swarm, J. Math. Biol. 38 (1999) 534–570.

[20] C. M. Topaz, A. L. Bertozzi, M. A. Lewis, A nonlocal continuum model for biological aggregation, Bull. Math. Bio. 68 (2006) 1601–1623.

[21] A. L. Bertozzi, J. A. Carrillo, T. Laurent, Blow-up in multidimensional aggregation equations with mildly singular interaction kernels, Nonlinearity 22 (3) (2009) 683–710.

[22] P. Degond, S. Motsch, Continuum limit of self-driven particles with orientation interaction, Math. Models Methods Appl. Sci. 18 (suppl.) (2008) 1193–1215.

[23] R. Eftimie, G. de Vries, M. A. Lewis, F. Lutscher, Modeling group formation and activity patterns in self-organizing collectives of individuals, Bull. Math. Biol. 69 (5) (2007) 1537–1566.

[24] R. Eftimie, G. de Vries, M. A. Lewis, Complex spatial group patterns result from different animal communication mechanisms, Proc. Natl. Acad. Sci. 104 (17) (2007) 6974–6979.

[25] R. Eftimie, G. de Vries, M. Lewis, Weakly nonlinear analysis of a hyperbolic model for animal group formation, J. Math. Biol. 59 (2009) 37–74.

[26] J. P. Newman, H. Sayama, Effect of sensory blind zones on milling behavior in a dynamic self-propelled particle model, Phys. Rev. E 78 (011913).

[27] H. Kunz, C. K. Hemelrijk, Simulations of the social organization of large schools of fish whose perception is obstructed, Appl. Anim. Behav. Sci. 138 (2012) 142–151.

[28] G. Albi, L. Pareschi, Binary interaction algorithms for the simulation of flocking and swarming dynamics, Multiscale Model. Simul. 11 (1) (2013) 1–29.

[29] F. Brauer, C. Castillo-Chavez, Mathematical Models in Population Biology and Epidemiology, Vol. 40 of Texts in Applied Mathematics, Springer, New York, 2001.

[30] S. Liu, E. Beretta, A stage-structured predator-prey model of Beddington-DeAngelis type, SIAM J. Appl. Math. 66 (4) (2006) 1101–1129.

[31] M. R. Myerscough, B. F. Gray, W. L. Hogarth, J. Norbury, An analysis of an ordinary differential equation model for a two-species predator-prey system with harvesting and stocking, J. Math. Biol. 30 (6) (1992) 389–411.

[32] M. Kuwamura, T. Nakazawa, T. Ogawa, A minimum model of prey-predator system with dormancy of predators and the paradox of enrichment, J. Math. Biol. 58 (3) (2009) 459–479.

[33] A. Okubo, Diffusion and Ecological Problems, Mathematical Models, Springer Verlag, New York, 1980.

[34] R. S. Cantrell, C. Cosner, Models for predator-prey systems at multiple scales, SIAM Rev. 38 (2) (1996) 256–286.

[35] S. Niizeki, Existence and stability of traveling wave solutions of competition models with migration effects, Japan J. Appl. Math. 6 (3) (1989) 421–478.

[36] E. Barbera, C. Curró, G. Valentia, Wave features of a hyperbolic prey-predator model, Math. Meth. Appl. Sci. 33 (2010) 1504–1515.

[37] K. Hadeler, Mathematics inspired by biology. Lecture Notes in Mathematics, Springer Verlag, 1999, Ch. Reaction transport systems in biological modelling, pp. 95–150.

[38] K. P. Robinson, M. J. Tetley, Behavioural observations of foraging minke whales (balaenoptera acutorostrata) in the outer moray firth, north-east scotland, J. Mar. Biol Ass. U.K. 87 (2007) 85–86.

[39] C. Canuto, M. Y. Hussaini, A. Quarteroni, T. A. Zang, Spectral methods in fluid dynamics, Springer Series in Computational Physics, Springer-Verlag, New York, 1988.

[40] P. Stander, Cooperative Hunting in Lions: The Role of the Individual, Behav. Ecol. Sociobiol. 29 (6) (1992) 445–454.

[41] P. Romanczuk, L. Schimansky-Geier, Swarming and pattern formation due to selective attraction and repulsion, Interface Focus 2 (6) (2012) 746–756.

[42] B. L. Partridge, Structure and function of fish schools, Scientific American 246 (6) (1982) 114–123.

[43] T. J. Pitcher, J. K. Parrish, Functions of shoaling behaviour in teleosts, Chapman & Hall, 1993.

[44] A. E. Magurran, The adaptive significance of schooling as an anti-predator defence in fish, Ann. Zool. Fennici 27 (1990) 51–66.

[45] G. Carey, J. M. Teal, J. W. Kanwisher, K. D. Lawson, J. S. Beckett, Warm-bodied fish, American Zoologist 11 (1971) 135–143.

[46] D. B. Grobecker, T. W. Pietsch, High-speed cinematographic evidence for ultrafast feeding in antennariid anglerfishes, Am. Ass. Adv. Sci. 205 (4411) (1979) 1161–1162.

[47] A. Kamimura, T. Ohira, Group chase and escape, New J. Phys. 12 (2010) 053013.

[48] M. W. Hayward, J. O'Brien, M. Hofmeyr, G. I. H. Kerley, Prey preferences of the african wild dog lycaon pictus (canidae: Carnivora): Ecological requirements for conservation, J. Mammalogy 87 (2006) 1122–1131.

[49] S. Camazine, J.-L. Deneubourg, N. R. Franks, J. Sneyd, G. Theraulaz, E. Bonabeau, Self-organization in biological systems, Princeton Studies in Complexity, Princeton University Press, Princeton, NJ, 2001.

[50] W. W. Murdoch, Switching in general predators: Experiments on predator specificity and stability of prey, Ecological Monographs 39 (4) (1969) 335–354.

[51] W. D. Hamilton, Geometry for the selfish herd, J. Theor. Biol. 31 (1971) 295–311.